Structural Relaxation around Cr^{3+} in $YAlO_3-YCrO_3$ Perovskites from Electron Absorption Spectra

Giuseppe Cruciani,*,† Matteo Ardit,† Michele Dondi,‡ Francesco Matteucci,‡ Magda Blosi,‡,§ Maria Chiara Dalconi,† and Stefania Albonetti§

Department of Earth Sciences, University of Ferrara, Via Saragat 1, 44100 Ferrara, Italy, Institute of Science and Technology for Ceramics (ISTEC−CNR), Via Granarolo 64, 48018 Faenza, Italy, and Department of Industrial Chemistry and Materials, University of Bologna, Via Risorgimento 4, 40136 Bologna, Italy

Received: May 8, 2009; Revised Manuscript Received: September 16, 2009

The structural relaxation around Cr^{3+} in $YAl_{1-x}Cr_xO_3$ perovskites was investigated and compared with analogous Cr−Al joins (corundum, spinel, garnet). Eight compositions ($x_{Cr^{3+}}$ from 0 to 1) were prepared by sol−gel combustion and were analyzed by a combined X-ray diffraction (XRD) and electron absorption spectroscopy (EAS) approach. The unit cell parameters and the XRD averaged octahedral (Cr,Al)−O and $^{[VIII]}$Y−O bond distances scale linearly with the chromium fraction. The optical parameters show an expected decrease of crystal field strength ($10Dq$) and an increase of covalency (B_{35}) and polarizability (B_{55}) toward $YCrO_3$, but a nonlinear trend outlines some excess $10Dq$ below $x_{Cr^{3+}} \sim 0.4$. The local Cr−O bond lengths, as calculated from EAS, indicate a compression from 1.98 Å ($x_{Cr^{3+}} = 1.0$) down to 1.95 Å ($x_{Cr^{3+}} = 0.035$) so that the relaxation coefficient of perovskite ($\varepsilon = 0.54$) is the lowest in comparison with garnet ($\varepsilon = 0.74$), spinel ($\varepsilon = 0.68$), and corundum ($\varepsilon = 0.58$) in contrast with its structural features. The enhanced covalent character of the $Cr^{3+}-O-Cr^{3+}$ bond in the one-dimensional arrangement of corner-sharing octahedra can be invoked as a factor limiting the perovskite polyhedral network flexibility. The increased probability of Cr−O−Cr clusters for $x_{Cr^{3+}}$ greater than ∼0.4 is associated to diverging trends of nonequivalent interoctahedral angles. The relatively low relaxation degree of $Y(Al,Cr)O_3$ can be also understood by considering an additional contribution to $10Dq$ because of the electrostatic potential of the rest of the lattice ions upon the localized electrons of the CrO_6 octahedron. Such an "excess" of $10Dq$ increases when the point symmetry of the Cr site is low, as in perovskite, and would be affected by the change of yttrium effective coordination number observed by XRD for $x_{Cr^{3+}}$ greater than ∼0.4. This would justify the systematic underestimation of local Cr−O bond distances, as inferred from EAS, compared to what is derived from X-ray absorption (XAS) studies implying a stronger degree of relaxation around Cr^{3+} of all the structures considered and supporting the hypothesis that $10Dq$ from EAS contains more information than previously retained particularly an additional contribution from the next nearest neighboring ions.

1. Introduction

Perovskites $^{[XII]}A^{3+[VI]}B^{3+}O_3$ are ternary compounds with an ideal cubic structure commonly visualized with the B-cell setting atomic model: the A-cations at the body centers, the B-cations at the cube corners, and the oxygens in the middle of the cube edges.[1] In this ideal case, the A−O/B−O ratio is equal to $\sqrt{2}$. In nonideal conditions, this ratio varies and the perovskite structure answers with a symmetry decreasing as a function of the chemical nature of A and B cations. For the $YCrO_3-YAlO_3$ system, the perovskite symmetry becomes orthorhombic (*Pnma* space group) with (Al, Cr) accommodated in a slightly distorted octahedral site and Y hosted in an eight-fold coordinated site.[1,2]

The peculiarity of these perovskites is their application in several fields, for example, optic-electrical in solid oxide fuel cells,[3] high-temperature electrode and thermoelectric materials,[4] or as ceramic pigment.[5−7] Analogously to what happens along the $Al_2O_3-Cr_2O_3$ join,[8,9] the color ranges from bright green ($YCrO_3$) to red ($YAl_{0.97}Cr_{0.03}O_3$) passing through almost uncolored compositions ($YAl_{0.87}Cr_{0.13}O_3$). Such chromatic changes depend on the shift of the main optical bands of Cr^{3+} ions occurring as a consequence of varying both crystal field strength ($10Dq$) and covalence degree of Cr−O bond.[9,10] According to the crystal field theory,[10,11] the $10Dq$ value depends on the metal−oxygen distance by a relationship that in the point charge approximation is close to the inverse fifth power of the mean distance <B−O>:

$$10Dq = 5/3 \cdot Q \cdot \langle r^4 \rangle \cdot <B-O>^{-5} \quad (1)$$

where both the effective charge on the ligands Q and the average radius of d orbitals $\langle r \rangle$ can be considered constant for the same metal ion in the same ligand environment; thus, this relation can be simplified as[11−13]

$$10Dq = \text{const} \cdot <B-O>^{-5} \quad (2)$$

However, the actual relationship of $10Dq$ with the B−O distance depends on the system with exponents typically in the −4 to −6 range.[14] Early studies have established that the point charge approximation (i.e., exponent −5) is obeyed by the perovskite-like compounds.[15] At the atomic scale, a structural

* To whom correspondence should be addressed. E-mail: cru@unife.it.
† University of Ferrara.
‡ ISTEC−CNR.
§ University of Bologna.

10.1021/jp9043072 CCC: $40.75
Published on Web 11/11/2009

relaxation associated with cation substitution affects the stability of binary solid solutions showing that the Vegard's law is not observed.[13,16] Several studies demonstrate that the local mean distances between the central ion and the surrounding oxygens of mineral solid solutions strongly deviate from what is obtained by the crystal-averaging diffraction methods. The reason stems from the local relaxation around the specific octahedral site occupied by more than one type of central ion different in size.[13,16–19]

As proposed by Urusov,[20] a relaxation coefficient ε can be calculated on a geometrical basis; in our case, it is given by

$$\varepsilon = (\langle Cr-O\rangle_x^{local} - \langle Al-O\rangle_{x=0})\cdot (\langle Cr-O\rangle_{x=1} - \langle Al-O\rangle_{x=0})^{-1} \quad (3)$$

where x is the fraction of chromium; the mean polyhedral distances $\langle Al-O\rangle_{x=0}$ and $\langle Cr-O\rangle_{x=1}$ are obtained by diffraction methods, whereas the local mean distance can be determined by means of eq 2 by optical spectroscopy[17–19]

$$\langle Cr-O\rangle_x^{local} = (\langle Cr-O\rangle_{x\approx 1}^{local})\cdot [(10Dq_{Cr^{3+}})_{x=1}/(10Dq_{Cr^{3+}})_x]^{1/5} \quad (4)$$

where $\langle Cr-O\rangle_{x\approx 1}^{local}$ is well approximated by $\langle Cr-O\rangle_{x=1}$, the distance in the Cr end member taken from the crystal structural data.[13,16] ε is usually calculated as infinite dilution ($\varepsilon_{\lim x Cr\to 0}$) of the metal ion in the solid solution.[13]

The relaxation coefficient is $\varepsilon = 0$ in the case of absent relaxation, which corresponds to the Vegard's straight line predicted by the virtual crystal approximation (VCA) model, while it is $\varepsilon = 1$ for full relaxation, which is the situation implied by the hard sphere (HS) model.[20,21]

The goal of this paper is to assess the relaxation coefficient ε around Cr^{3+} in the $Y(Cr,Al)O_3$ perovskite series through a combined X-ray diffraction (XRD) and electron absorption spectroscopy (EAS) study. The discussion will be addressed to crystal structural constraints on relaxation by comparing analogous investigations on other Cr−Al joins, such as eskolaite-ruby,[8,22–24] grossular-uvarovite,[17,19] and spinel-magnesiochromite,[22] taking into account recent criticism to this approach on the basis of X-ray absorption (XAS) studies and ab initio electronic structure calculations. This insight into the interdependence of color on crystal structure is a key point to understand in depth the color mechanism and to design new and more efficient pigments exploiting the different chromatic spectra from the chromium end member (green) to the Cr-doped aluminum end member (red).

2. Experimental Section

2.1. Synthesis. Samples were prepared by sol−gel combustion, a technique combining the polymeric gel action with the fast combustion reaction, which is suitable to synthesize multicomponent systems in which the stoichiometry must be strictly maintained.[25] Eight samples were synthesized with an increasing chromium content to cover all the $YAlO_3-YCrO_3$ join (Table 1). $Al(NO)_3\cdot 9H_2O$ (98+%), $Y(NO)_3\cdot 6H_2O$ (99.9%), $Cr(NO)_3\cdot 9H_2O$ (99%), NH_4NO_3 (99%), anhydrous citric acid (99.5%), and NH_4OH (all purchased from Sigma-Aldrich) were used as precursors. The two steps involved in this technique, xerogel formation and combustion, are described in detail by Blosi et al.[26] The combusted precursor, a black fluffy powder, was ball milled in ethanol for 24 h, was sieved under 75 μm, and was calcined in an electric kiln at 1300 °C in static air (200 °C/h heating rate, 4 h soaking time, natural cooling) in an unsealed alumina crucible.

2.2. X-ray Powder Diffraction and Rietveld Refinements. X-ray powder diffraction was performed at room temperature using a Bruker D8 Advance diffractometer equipped with a Si(Li) solid state detector set to select Cu $K\alpha_{1,2}$ radiation. Data collection parameters were 15−130°2Θ measuring range, scan rate 0.02°2Θ, 10 s per step. The structural refinements were performed by the Rietveld method with the GSAS-EXPGUI software package.[27,28] The presence of impurity phases was accounted for by carrying out multiphase refinements in which only the scale factors and the cell parameters were varied for all phases except perovskite. Agreement factors of refinements are reported in Table 1. Starting atomic parameters for the orthorhombic perovskite were taken from Cruciani et al.[2] adopting the *Pnma* space group in nonstandard setting. Depending upon the number of impurities, the refined variables ranged up to 42 independent variables including scale factors, zero-point, 15 coefficients of the shifted Chebyschev function to fit the background, perovskite cell dimensions, atomic positions, and isotropic atomic displacement parameters. The line shape was described by a pseudo-Voigt function with the following refinable coefficients: three Gaussian terms (G_u, G_v, G_w), two Lorentzian terms (L_x, L_y), *S/L* (*S*: sample size; *L*: distance between sample and detector) and *H/L* (*H*: detector height; *L*: distance between sample and detector) to account for profile asymmetry due to axial divergence, and six terms for the anisotropic peak broadening (L_{11}, L_{22}, L_{33}, L_{12}, L_{13}, L_{23}).

2.3. Optical Spectroscopy. Electron absorption spectroscopy (EAS) was performed at room temperature by diffuse reflectance (Perkin-Elmer λ35 spectrophotometer, 300−1100 nm range, 0.03 nm step size, $BaSO_4$ integrating sphere, white reference material: $BaSO_4$ pellet). Reflectance (R_∞) was converted to absorbance (*K/S*, *K*: absorption; *S*: scattering) by the Kubelka−Munk equation: $K/S = 2(1 - R_\infty)\cdot(2R_\infty)^{-1}$.[12] The main absorbance bands in the optical spectra were deconvoluted (PFM, OriginLab) in order to obtain energy (centroid), band splitting (full width at half-maximum, fwhm), and optical density (area). The experimental errors, including background correction and reproducibility, are around 2% (energy), 5% (fwhm), and 10% (area). Crystal field strength 10*Dq* was calculated by fitting the energy of spin-allowed transitions in the d^3 Tanabe−Sugano diagram.[10,29] Interelectronic repulsion Racah parameters were calculated by spin-allowed (B_{35}) or spin-forbidden transitions (B_{55} and C).[30,31] The correspondent nephelauxetic ratios β_{35} and β_{55} were calculated as $\beta = B/B_0$, where B is experimental and B_0 is the value of the free ion. They are considered to express the covalent degree (β_{35}) and polarizability (β_{55}) of the Cr−O bonding.[21,30]

3. Results and Discussion

3.1. Crystal Structure. The amount of perovskite varies from 100% (the end members Cr1000 and Cr0 as well as the sample Cr750) to a minimum of 93.7% in the sample Cr75 (Table 1). This implies that samples with intermediate composition (i.e., from Cr500 to Cr35) are not strictly monophasic but contain minor phases, such as yttrium oxide (Y_2O_3) and two kinds of yttrium−aluminum oxides: YAG ($Y_3Al_5O_{12}$) and YAM ($Y_4Al_2O_9$). The occurrence of secondary phases (2.4% on average) has no significant effects on the incorporation of Cr^{3+} in the dominant perovskite phase because both Y_2O_3 and YAM have no octahedral sites in which Cr^{3+} could be accommodated, while YAG is well-known to host essentially a small amount

TABLE 1: Batch and Phase Composition, X-ray Diffraction Details, Unit Cell Parameters, Metal−Oxygen Distances, Site Distortion, and Effective Volume and Coordination Number of Polyhedra in Perovskite Structures Analyzed[a]

sample label	Cr1000	Cr750	Cr500	Cr250	Cr135	Cr75	Cr35	Cr0
				Batch Composition (Molar Ratios) and Color of Powders				
Cr/(Cr+Al)	1.000	0.750	0.500	0.250	0.135	0.075	0.035	0.000
color	deep green	green	green	light green	gray	pink	pink	white
				Quantitative Phase Analysis				
perovskite (% wt)	100.0(0)	100.0(0)	97.6(1)	98.3(1)	97.0(1)	93.7(1)	97.0(1)	100.0(1)
				other phases (% wt):				
Y_2O_3			2.4(1)					
$Y_4Al_2O_9$				1.7(1)		4.6(1)	1.4(1)	
$Y_3Al_5O_{12}$					3.0 (1)	1.7(1)	1.6(1)	
				Agreement Factors and Refinement Details				
R_{wp}	0.159	0.172	0.132	0.127	0.141	0.137	0.143	0.150
R_p	0.106	0.130	0.089	0.083	0.099	0.100	0.105	0.105
no. of data	6000	5749	4749	4749	4749	5749	5749	6000
R_F^2	0.066	0.074	0.040	0.041	0.049	0.064	0.069	0.071
no. of reflections	402	398	283	281	279	384	383	380
no. of variables	27	28	32	32	30	42	42	27
				Unit Cell Parameters				
a (Å)	5.5242(1)	5.4815(1)	5.4316(1)	5.3833(1)	5.3581(1)	5.3458(1)	5.3356(1)	5.3298(1)
b (Å)	7.5356(1)	7.4973(1)	7.4534(1)	7.4140(1)	7.3929(1)	7.3844(1)	7.3763(1)	7.3724(1)
c (Å)	5.2434(1)	5.2306(1)	5.2137(1)	5.1983(1)	5.1895(1)	5.1858(1)	5.1820(1)	5.1806(1)
unit cell volume (Å^3)	218.27	214.96	211.07	207.48	205.56	204.71	203.95	203.57
				Chromium Fraction				
$x(Cr^{3+})$	1.00	0.73(1)	0.48(1)	0.24(1)	0.13(1)	0.06(1)	0.02(1)	0.00
probability of Cr−O−Cr bonds (%)	100	56	25	6	2	0.6	0.1	0
				Metal−Oxygen Mean Distances (Å)				
$^{[VIII]}$A−O	2.417	2.414	2.410	2.406	2.404	2.403	2.402	2.402
$^{[XII]}$A−O	2.738	2.718	2.696	2.676	2.666	2.661	2.656	2.655
$^{[VI]}$B−O	1.984	1.967	1.946	1.929	1.920	1.917	1.912	1.911
				Distortion Indices of Site A (Δ_8) and Site B (Δ_6) and Tolerance Factor				
Δ_8	4.448	3.933	3.408	3.107	3.046	3.086	2.928	2.925
Δ_6	0.044	0.056	0.066	0.046	0.064	0.062	0.039	0.048
$^{(VIII)}t_0$	0.861	0.868	0.876	0.882	0.885	0.886	0.888	0.889
				Polyhedral Volume, V (Å^3), and Effective Coordination Number, ECoN, of Site A				
V_A	23.52	23.30	23.04	22.78	22.64	22.57	22.53	22.52
V_B	10.40	10.14	9.82	9.57	9.44	9.39	9.32	9.3
$ECoN_A$	6.59(4)	6.67(5)	6.84(2)	6.91(2)	6.94(3)	6.91(4)	6.95(4)	7.00(5)

[a] Figures in parentheses are standard deviations in the last decimal figure. R_F^2 is only referred to perovskite reflections. The distortion indices are defined by

$$10^3 \cdot \frac{\sum_{i:1}^{n} ((M-O)_i - \langle M-O \rangle)^2}{n \cdot (\langle M-O \rangle)^2}$$

The observed tolerance factor is $^{(VIII)}t_0 = {}^{[VIII]}A-O/[2^{1/2}(^{[VI]}B-O)]$. The effective coordination number is defined as $ECoN = \Sigma_i w_i$ (i), where $w_i = \exp[1 - (l_i/l_{av})^6]$ (ii) is called the "bond weight" of the ith bond. In eq ii, l_{av} represents a weighted average bond length defined as $l_{av} = (\Sigma_i l_i \exp[1 - (l_i/l_{min})^6]) (\Sigma_i \exp[1 - (l_i/l_{min})^6])^{-1}$ (iii), where l_{min} is the smallest bond length in the coordination polyhedron.

of Cr^{4+} in fourfold coordination.[32,33] This is confirmed by the refined chromium fractions reported in Table 1 ($x_{Cr^{3+}}$) which are very close to the designed values in batch compositions.

The unit cell parameters (*a*-, *b*-, and *c*-cell edges and cell volume) scale linearly with the refined chromium fraction ($x_{Cr^{3+}}$) along the $YAlO_3-YCrO_3$ join (Figure 1) in apparent agreement with Vegard's law. Analogously, both the average octahedral <Cr,Al−O> and the $<^{[VIII]}Y-O>$ bond distances, the latter being averaged on the shortest eight Y−O distances, show linear and positive trends with $x_{Cr^{3+}}$ (Figure 2). Such a parallel behavior of <A−O> and <B−O> is opposite to what is observed in the series of $(Y,REE)AlO_3$ perovskites, where an increase of the $<^{[VIII]}A-O>$ distance, because of incorporation of larger REE ions in the A site, is associated to a decrease of the <B−O> distance resulting in a partial conservation of the unit cell volume.[2] A similar mechanism is not effective along the $YAlO_3-YCrO_3$ join likely because of the narrower range of bond distance variation. This is evident from the relatively small changes of the polyhedral volumes of both the A and B sites (Table 1) whose ratio shows that the volume increasing of $(Cr,Al)O_6$ octahedra, connected with the increased ionic radius from Al^{3+} (0.535 Å) to Cr^{3+} (0.615 Å),[34] is only ∼5% more than that of YO_8 polyhedra. This suggests that the octahedral volume expansion is not directly transferred to the whole unit cell, but it is partially compensated by the well-known tilting phenomena occurring in perovskites.[1] The observed change of <A−O> and <B−O> distances is also seen in the linear decrease of the tolerance factor (see Table 1) suggesting that $Y(Al,Cr)O_3$ perovskites become more distorted from the cubic prototype with the increase of $x_{Cr^{3+}}$. Figure 2b shows the change of (Al,Cr)−$O_{1,2}$−(Al,Cr) bond angles along the studied $YAlO_3-YCrO_3$ join. The two symmetrically nonequivalent bond

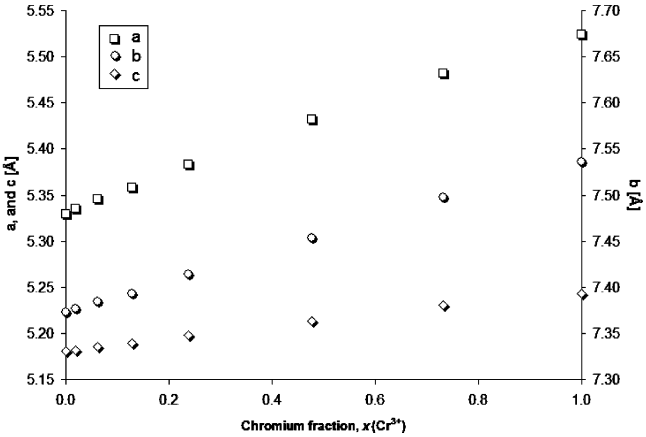

Figure 1. Variation of the unit cell parameters as a function of the refined chromium fraction ($x_{Cr^{3+}}$).

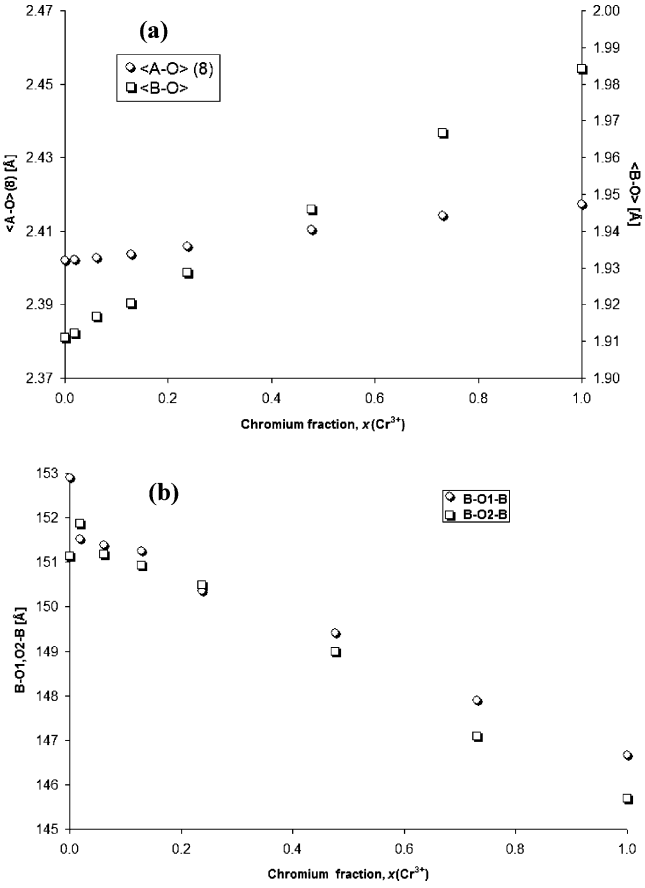

Figure 2. Variation of (a) mean metal−oxygen distances and (b) $B-O_{1,2}-B$ bond angles as a function of refined chromium fraction, $x_{Cr^{3+}}$.

angles vary in a similar way up to a Cr fraction close to 0.4 while their trends start to diverge above this value. Another important feature, which occurs along the $YAlO_3-YCrO_3$ join when the chromium content increases above approximately $x_{Cr^{3+}} = 0.4$, is the significant change of the effective coordination number (ECoN) of yttrium ions in the A site (Figure 3). The ECoN parameter is particularly useful to reveal the subtle variations of the effective charge contribution that each ligand provides to the coordination shell of a central cation.[35,36] It appears from Figure 3 that the sevenfold effective coordination of Y gradually decreases as a function of Cr^{3+} content reaching a value of 6.5 in the $YCrO_3$ end member. The rate of decrease is larger above $x_{Cr^{3+}} = 0.4$. This suggests the existence of a

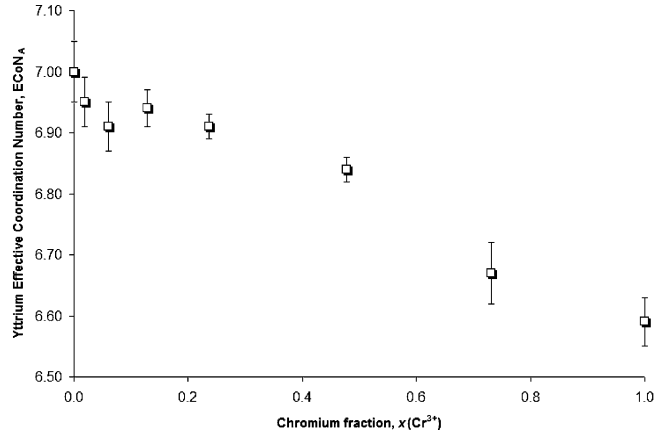

Figure 3. Variation of the effective coordination number of yttrium ions in function of the refined chromium fraction ($x_{Cr^{3+}}$).

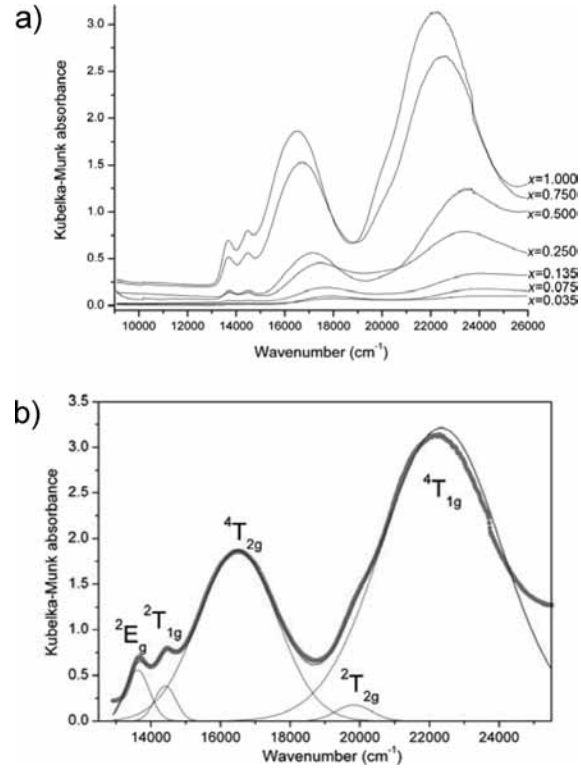

Figure 4. Diffuse reflectance spectra of $Y(Cr,Al)O_3$ perovskites (a) and example of spectrum deconvolution (b).

threshold value above which the lattice strain induced by the incorporation of Cr^{3+} in the octahedral sites of $YAlO_3$ can no longer be accommodated by octahedral expansion and the strain is released by a more significant rearrangement of the A-site coordination environment.

3.2. Optical Properties. $Y(Cr,Al)O_3$ perovskites exhibit the typical optical spectra of Cr^{3+} in octahedral coordination (Figure 4a) involving d−d electronic transitions.[17–19,37,38] Band absorbance increases almost linearly with $x_{Cr^{3+}}$, while band energy undergoes a gradual shift because of the changing crystal field strength along the $YAlO_3-YCrO_3$ join.[10,12,31]

The most intense bands are attributed to the parity-forbidden and spin-allowed transitions from the ground level $^4A_{2g}$ (^4F) to $^4T_{2g}$ (^4F) and $^4T_{1g}$ (^4F) at 16 000−18 000 cm^{-1} and 22 000−24 000 cm^{-1}, respectively. Minor bands, because of the parity- and spin-forbidden transitions $^4A_{2g}$ (^4F) → ^2E_g (^2G), → $^2T_{1g}$ (^2G), and → $^2T_{2g}$ (^2G), are observed at approximately 13 700 cm^{-1}, 14 300 cm^{-1}, and 19 500 cm^{-1}, respectively. Diffuse reflectance spectra

TABLE 2: Energy (Peak), Band Splitting (fwhm), and Intensity (Area) of the Optical Bands of Cr^{3+} in Y(Cr,Al)O_3 Perovskites

	$^4A_{2g}$ →	→ $^4T_{2g}$ (^4F)			→ $^4T_{1g}$ (^4F)			→ ^2E_g (^2G>)	→ $^2T_{1g}$ (^2G)	→ $^2T_{2g}$ (^2G)
sample	$x_{Cr^{3+}}$	peak (cm^{-1})	fwhm (cm^{-1})	area (au)	peak (cm^{-1})	fwhm (cm^{-1})	area (au)	peak (cm^{-1})	peak (cm^{-1})	peak (cm^{-1})
Cr35	0.02	17 870	1920	40	24 100	3150	50	13 745	14 795	19 415
Cr75	0.06	17 880	2240	150	23 910	4070	250	13 735	14 570	19 520
Cr135	0.13	17 610	2160	220	23 695	2900	340	13 715	14 435	19 540
Cr250	0.24	17 340	2130	310	23 240	2930	1010	13 750	14 435	19 280
Cr500	0.48	16 980	2285	740	23 110	3310	4140	13 720	14 435	19 380
Cr750	0.73	16 630	2100	2390	22 410	3010	5730	13 695	14 385	20 080
Cr1000	1.00	16 410	2140	3190	22 140	2960	7030	13 640	14 360	20 215

TABLE 3: Optical Parameters of Cr^{3+} in Y(Cr,Al)O_3 Perovskites: Crystal Field Strength (10*Dq*), Interelectronic Repulsion Racah B_{35}, B_{55}, and C Parameters, Nephelauxetic Ratios β_{35} and β_{55}, and Local Cr−O Distance Calculated by Eq 2

sample	$x_{Cr^{3+}}$	10*Dq* (cm^{-1})	B_{35} (cm^{-1})	B_{55} (cm^{-1})	C (cm^{-1})	β_{35} (1)	β_{55} (1)	<Cr−O>^{local} (Å)
Cr35	0.02	17 867	609	805	2883	0.66	0.88	1.950 ± 0.005
Cr75	0.06	17 864	588	790	2904	0.64	0.86	1.950 ± 0.005
Cr135	0.13	17 616	593	787	2928	0.65	0.86	1.956 ± 0.005
Cr250	0.24	17 349	573	811	2886	0.62	0.88	1.962 ± 0.005
Cr500	0.48	16 968	576	797	2899	0.63	0.87	1.971 ± 0.005
Cr750	0.73	16 627	565	686	3060	0.62	0.75	1.979 ± 0.006
Cr1000	1.00	16 405	560	654	3116	0.61	0.71	1.984 ± 0.006

were successfully deconvoluted using five Gaussian bands for the Cr^{3+} transitions (Figure 4b) whose values of energy, splitting, and optical density are listed in Table 2.

The main optical parameters, calculated on the basis of the Cr^{3+} transitions energy, are reported in Table 3. The crystal field strength 10*Dq* decreases regularly with $x_{Cr^{3+}}$, but its trend is not linear all along the join (Figure 5a). In good agreement with results from XRD analysis (e.g., variation of B−$O_{1,2}$−B angles and $ECoN_A$), we interpret the 10*Dq* versus $x_{Cr^{3+}}$ relationship on the basis of two linear trends changing their slopes at approximately $x_{Cr^{3+}} = 0.4$. This fact, already observed in the corundum−eskolaite join,[21] is attributable to different slopes versus $x_{Cr^{3+}}$ of the three components in which the $^4A_{2g}$→$^4T_{2g}$ (O_h) transition is split (^4A→^4A, ^4A→^4A, ^4A→^4A) as a consequence of the low point symmetry (C_1) of the octahedral site in the orthorhombic perovskite lattice. However, such splitting of the main Cr^{3+} band is too small to be appreciable in terms of bandwidth in diffuse reflectance spectra (e.g., König−Kremer[39] diagrams). As a matter of fact, fwhm values of $^4T_{2g}$ and $^4T_{1g}$ transitions remain almost constant all along the join (Table 2) as the distortion Δ_6 randomly fluctuates from 0.04 to 0.07 (Table 1).

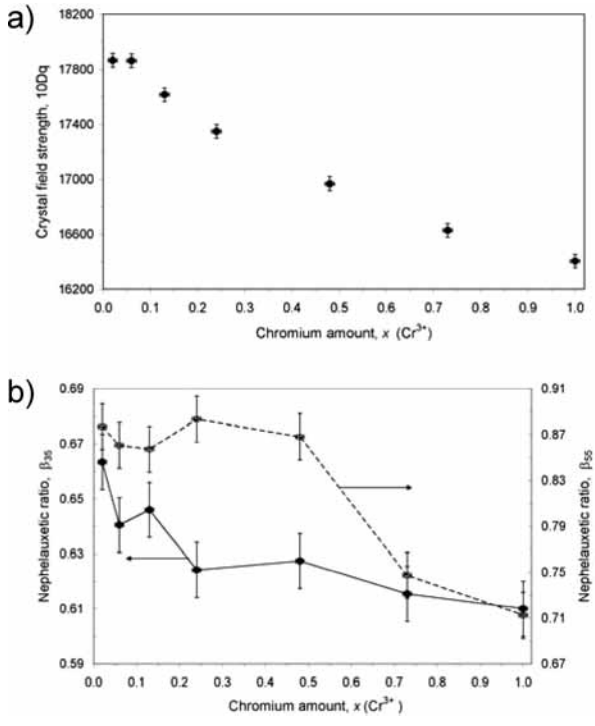

Figure 5. Variation along the $YAlO_3$−$YCrO_3$ join of (a) crystal field strength 10*Dq* and (b) Racah B_{35} and B_{55} parameters.

The Racah parameters exhibit similar trends versus $x_{Cr^{3+}}$ (Figure 5b). The nephelauxetic ratio β_{55} rapidly increases from Cr1000 (0.71) to Cr500 (0.87) and then remains stable fluctuating in the 0.86−0.88 range toward Cr0. These high β_{55} values imply relatively strong π-bonds for Cr−O in perovskite,[22] although a diminished polarizability of oxygens around Cr^{3+} in the Al-rich terms may be also invoked for analogy with other Al−Cr oxides.[13] Both reasons are consistent with the known magnetic ordering of Cr−Cr pairs in orthochromates persisting down to Cr750 compositions.[40] On the other hand, the nephelauxetic ratio β_{35} increases rather regularly from 0.61 (Cr1000) to 0.66 (Cr35); this limited variation of β_{35} confirms preliminary literature data on yttrium chromium perovskites[22] and demonstrates the assumption in eq 2 that the constant retains its value.[13,16] Such a growing trend of β_{35} indicates a slightly reduced covalency of the Cr−O bonding, which has been also observed along other Cr−Al joins, such as Cr_2O_3−Al_2O_3[8,22] and $MgCr_2O_4$−$MgAl_2O_4$.[22] Overall, the covalent degree of the Cr−O bonding in Y(Cr,Al)O_3 perovskites is higher ($0.61 < \beta_{35} < 0.66$) with respect to the spinel $MgCr_2O_4$−$MgAl_2O_4$ series ($0.69 < \beta_{35} < 0.73$)[20] and the garnet $Ca_3Cr_2Si_3O_{12}$−$Ca_3Al_2Si_3O_{12}$ join ($0.69 < \beta_{35} < 0.77$),[17,19] but it falls within the wide variation range ($0.50 < \beta_{35} < 0.72$) of the Cr_2O_3−Al_2O_3 join.[8,9,22−24]

3.3. Structural Relaxation. The local Cr−O mean bond lengths were calculated from electronic absorption spectra according to eq 4, and these results are listed in Table 3. The relaxation of the perovskite structure around Cr^{3+} can be appreciated plotting <Cr−O>^{local} versus $x_{Cr^{3+}}$ (Figure 6a). The relaxation coefficient, calculated according to eq 3, yields $\varepsilon_{limxCr\to 0} = 0.54$, which implies a degree of structural relaxation approximately halfway between the HS and the VCA models. Such a relatively low relaxation coefficient does not necessarily imply that the perovskite structure behaves as an inflexible one.

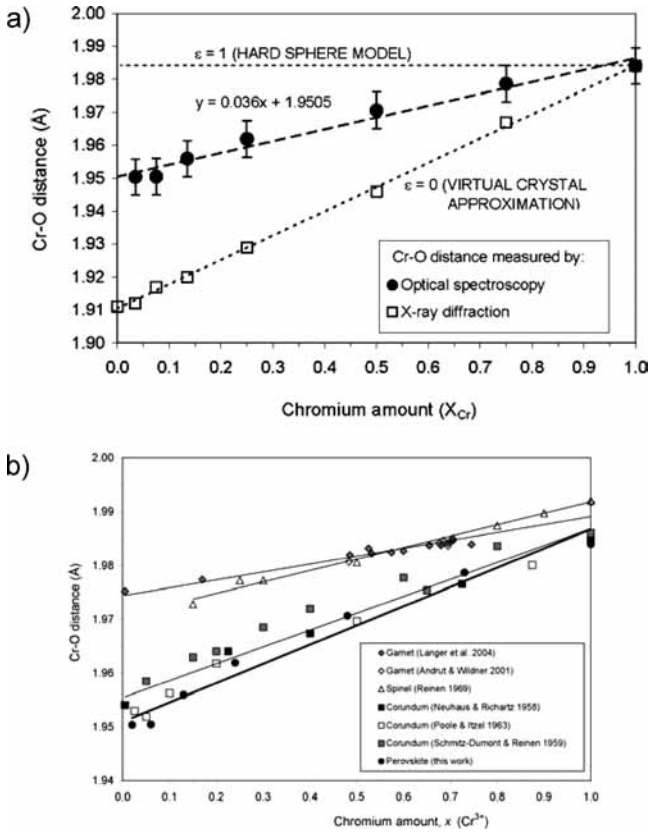

Figure 6. Coefficient of structural relaxation around Cr^{3+} in the $Y(Cr,Al)O_3$ perovskites (a) and comparison with other crystal structures (b).

Perovskites are known to display very large structural flexibility.[1] Comparison with other dense oxide structures will help to clarify this issue.

As a matter of fact, the value found here for the ε coefficient in $Y(Cr,Al)O_3$ perovskites is the lowest among $(Al,Cr)O_6$ polyhedra as appreciable by comparison with the well-studied series of uvarovite−grossular,[17,19] magnesiochromite−spinel,[22] and eskolaite−corundum.[8,22–24] Available EAS data allow the calculation of the correspondent value of $\varepsilon_{\lim x Cr \to 0}$, which is 0.74 for garnet, 0.68 for spinel, and 0.58 for corundum (Figure 6b). This ranking can be interpreted as because of a progressive decrease of polyhedral network flexibility when moving from garnet (isolated octahedra, edge-shared to tetrahedra), to spinel (edge-sharing octahedra, corner-shared to tetrahedra), to corundum (corner-, edge-, and face-sharing octahedra). More in detail, Juhin et al.[41] concluded that a complete relaxation in pyrope is achieved through deformation of MgO_8 dodecahedra and SiO_4 tetrahedra, the former to a greater extent, which surround the central CrO_6 octahedron. On the other hand, bond buckling and angular tilts of Mg-centered tetrahedra around the CrO_6 octahedra have been recognized as the strain-accommodating mechanism in spinel,[42] while the extension of the relaxation process up to the second shell has not been observed in corundum because of the reduced degrees of freedom of its structure.[43]

From a purely geometrical point of view, the polyhedral connectivity in the perovskite network (corner-sharing octahedra) would suggest a relatively large flexibility as also testified by the complex tilting systems and the ability to host a large variety of elements well-known for this structure.[1] This appears to be somewhat in contrast with the lowest ε value found in the $Y(Cr,Al)O_3$ perovskites under study. However, it has been suggested that the presence of M−O−M (e.g., M = a transition-metal ion) one-dimensional chains formed by corner-sharing octahedra in perovskites will lead to an enhanced covalency accompanying the M3d−O2p hybridization thus explaining the large discrepancies found between observed and calculated total polarizabilities.[44] Such an enhanced covalency can also act as a constraint on the M−O−M bond angle limiting to some extent the degrees of freedom in the perovskite network. The probability of occurrence of Cr−O−Cr bridges has been calculated under the assumption of random distribution for Cr^{3+} in $Y(Al,Cr)O_3$ (see Table 1). Interestingly, the nonlinear relationship of probability versus $x_{Cr^{3+}}$ (plot not shown here) can be approximated by two linear trends changing their slopes at $x_{Cr^{3+}} \sim 0.4$. Cr−O−Cr clusters can be responsible for the diverging trends of $B-O_{1,2}-B$ bond angles observed in Figure 2b for $x_{Cr^{3+}}$ greater than ∼0.4. They will act as a local structural constraint forcing the O1 and O2 hinges of octahedral chains to be no longer equivalent.

To better understand the significance of the EAS-based ε value found in our work, we recall some recent papers[45–47] disclosing that the crystal field strength relationship expressed in eq 2 is better defined as the sum of two terms: the first is actually the $10Dq$ as given in eq 2, while the second, $V_R(\mathbf{r})$, accounts for the electrostatic potential of the rest of the lattice ions upon the localized electrons of the CrO_6 octahedron.[46] Under the assumption that this additional term depends on the distance between Cr and neighboring ions by a power law R^{-5}, it is reasonable to suppose that the main contribution comes from the first two shells and particularly from the Y ions lying at 3.0−3.4 Å from the (Al,Cr) position. This additional contribution was observed to increase when the point symmetry of the Cr site decreased,[45] and it is largely affected by the covalency of the Cr−O bond[46] also mentioned above. In particular, the polarization-dependent part of $V_R(\mathbf{r})$ is associated to a change in covalency of the Cr−O bonding,[46] which is in line with the conclusions reached on the basis of combined EAS and XAS results on the corundum−eskolaite join.[9] Following this line of reasoning, the as-measured $10Dq$ values should be subtracted by a correction term equal to $V_R(\mathbf{r})$ before being used for calculation of the local Cr−O bond distances. The larger derived distances lead to a greater calculated relaxation coefficient.

This interpretation would justify the systematic underestimation of local Cr−O bond distances as inferred from optical spectra compared to what is derived from XAS studies.[41–43] As a consequence, the ε coefficients calculated by extended X-ray absorption fine structure (EXAFS) (∼1 for garnet,[41] 0.83 for spinel,[42] 0.76 for corundum,[9,43] and ∼0.8 for perovskite[48]) are larger than the ones calculated by EAS implying a stronger degree of relaxation around Cr^{3+} of all the structures considered. The relaxation ranking defined by XAS corresponds to that given by EAS but for the perovskite series. Interestingly, a perfect correspondence should be obtained if the relaxation coefficient of $Y(Cr,Al)O_3$ would be calculated by using the samples from Cr1000 to Cr250: in this case, the resulting $\varepsilon = 0.61$ is intermediate between those of corundum and spinel. It is significant that samples from Cr250 to Cr35, showing an "excess" of crystal field strength responsible for the nonlinearity of the relationship $x_{Cr^{3+}}$ versus $10Dq$ (Figure 5a), are characterized by a different arrangement of the second nearest neighbors, that is, yttrium effective coordination number close to 7 (Figure 3), which is likely to play an appreciable effect on the electrostatic potential $V_R(\mathbf{r})$.

The discrepancies between EAS and XAS data have induced a vivacious discussion and a criticism about the capacity of EAS

to determine the actual Cr−O local distances[9,41,42] and about the ligand field theory to describe accurately the electronic properties of transition-metal impurities in wide gap materials.[45–47] The picture arising from our study substantially confirms that the local Cr−O distances and the related ε relaxation coefficients, as measured by EAS, are not reliable in absolute terms but should be used to compare different structures. The crystal field strength derived from electron absorption spectra appears to contain more information than previously retained particularly an additional contribution from the second nearest neighboring ions, for example, yttrium in the $Y(Cr,Al)O_3$ perovskites.

4. Conclusions

The expected decrease of crystal field strength along the $YAlO_3-YCrO_3$ join occurs with a nonlinear trend suggesting a change of chromium environment toward the Al end term with some excess 10*Dq* with respect to what is predictable by the tendency constructed with samples Cr1000→Cr250. The local Cr−O bond lengths, as calculated from EAS, go from 1.98 Å (Cr1000) down to 1.95 Å (Cr35) indicating an unexpectedly low relaxation coefficient of perovskite ($\varepsilon = 0.54$) in comparison with garnet ($\varepsilon = 0.74$), spinel ($\varepsilon = 0.68$), and corundum ($\varepsilon = 0.58$) whose ranking is connected with a progressive decrease of polyhedral network flexibility. The low relaxation of perovskite network is explained by the increased probability of covalent-enhanced $Cr^{3+}-O-Cr^{3+}$ bonds for $x_{Cr^{3+}}$ greater than ~0.4; the occurrence of Cr−O−Cr clusters is responsible for the diverging trends of nonequivalent (Al,Cr)−O−(Al,Cr) angles and the change of yttrium coordination. Considering now the systematic underestimation of local Cr−O bond distances inferred from EAS, compared to those from XAS, an additional contribution to 10*Dq* originating from the electrostatic potential of the rest of the lattice ions upon the localized electrons of the CrO_6 octahedron has to be invoked. This interpretation would justify the excess 10*Dq*, coming from a changed electronic potential on Cr^{3+} ions, because of a variation of the yttrium effective coordination number close to the $YAlO_3$ end term. This effect is enhanced in perovskites because of the low point symmetry of the Cr site. These results support the hypothesis that electron absorption spectra, as well as crystal field strength values derived from them, contain more information than previously acknowledged especially some additional contribution to the electronic potential from the next nearest neighboring ions. However, further investigations are needed, particularly criss-crossing structural (XRD) and spectroscopic data (XAS, EAS) with ab initio electronic structure calculations.

References and Notes

(1) Mitchell, R. H. *Perovskites: Modern and Ancient*; Almaz Press: Thunder Bay, Ontario, Canada, 2002.
(2) Cruciani, G.; Matteucci, F.; Dondi, M.; Baldi, G.; Barzanti, A. *Z. Kristallogr.* **2005**, *220*, 930.
(3) Tachiwaki, T.; Kunifusa, Y.; Yoshinaka, M.; Hirota, K.; Yamaguchi, O. *Int. J. Inorg. Mater.* **2001**, *3*, 107.
(4) Armstrong, T. R.; Stevenson, J. W.; Hasinska, K.; McCready, D. E. *J. Electrochem. Soc.* **1998**, *145*, 4282.
(5) Baldi, G.; Dolen, N. *Mater. Eng.* **1999**, *10*, 151.
(6) Marinova, Y.; Hohemberger, J. M.; Cordoncillo, E.; Escribano, P.; Carda, J. B. *J. Eur. Ceram. Soc.* **2003**, *23*, 213.
(7) Matteucci, F.; Lepri Neto, C.; Dondi, M.; Cruciani, G.; Baldi, G.; Boschi, A. O. *Adv. Ceram. Appl.* **2006**, *105*, 99.
(8) Poole, C. P.; Itzel, J. F. *J. Chem. Phys.* **1963**, *39*, 3445.
(9) Gaudry, É.; Sainctavit, P.; Juillot, F.; Bondioli, F.; Ohresser, P.; Letard, I. *Phys. Chem. Miner.* **2006**, *32*, 710.
(10) Burns, R. G. *Mineralogical Applications of Crystal Field Theory*, 2nd ed.; Cambridge University Press: Cambridge, U.K., 1993.
(11) Dunn, T.; McClure, D. S.; Pearson, R. G. *Some aspects of crystal field theory*; Harper and Row: New York, 1965.
(12) Marfunin, S. *Physics of Minerals and Inorganic Materials*; Springer: Berlin, Germany, 1979.
(13) Langer, K. *Z. Kristallogr.* **2001**, *216*, 87.
(14) Moreno, M.; Barriuso, M. T.; Aramburu, J. A.; García-Fernandez, J. M.; García-Lastra, J. M. *J. Phys.: Condens. Matter* **2006**, *18*, R315.
(15) Poole, C. P. *J. Phys. Chem. Solids* **1964**, *25*, 1169.
(16) Galoisy, L. *Phys. Chem. Miner.* **1996**, *23*, 217.
(17) Langer, K.; Platonov, A. N.; Matsyuk, S. S. *Z. Kristallogr.* **2004**, *219*, 272.
(18) Taran, M. N.; Langer, K.; Abs-Wurmbach, I.; Frost, D. J.; Platonov, A. N. *Phys. Chem. Miner.* **2004**, *31*, 650.
(19) Andrut, M.; Wildner, M. *Am. Mineral.* **2001**, *86*, 1219.
(20) Urusov, V. S. *J. Solid State Chem.* **1992**, *98*, 223.
(21) Andrut, M.; Wildner, M.; Rudowicz, C. Z. *Optical Absorption Spectroscopy in Geosciences. Part II: Quantitative aspects of crystal fields*; Beran, A., Libowitzky, E., Eds.; EMU Notes in Mineralogy; Eötvös University Press: Budapest, Hungary, 2004; Vol. 6, p 145.
(22) Reinen, D. *Struct. Bonding (Berlin)* **1969**, *6*, 30.
(23) Schmidt-DuMont, O.; Reinen, D. *Z. Elektrochem.* **1959**, *63*, 978.
(24) Neuhaus, A.; Richartz, W. *Angew. Chem.* **1958**, *70*, 430.
(25) Montanari, G.; Costa, A. L.; Albonetti, S.; Galassi, C. *J. Sol-Gel Sci. Technol.* **2005**, *36*, 203.
(26) Blosi, M.; Albonetti, S.; Costa, A. L.; Dondi, M.; Ardit, M.; Cruciani, G. *J. Sol-Gel Sci. Technol.* **2009**, *50*, 449. DOI: 10.1007/s10971-009-1906-5.
(27) Larson, A. C.; Von Dreele, R. B. *General structure analysis system (GSAS)*; Los Alamos National Laboratory Report LAUR: Los Alamos, NM, 2000.
(28) Toby, B. H. *J. Appl. Crystallogr.* **2001**, *3*, 4–210.
(29) Tanabe, Y.; Sugano, S. *J. Phys. Soc. Jpn.* **1954**, *9*, 753.
(30) Lever, A. B. P. *Inorganic Electronic Spectroscopy*, 2nd ed.; Elsevier: Amsterdam, 1984.
(31) Wildner, M.; Andrut, M.; Rudowicz, C. Z. *Optical Absorption Spectroscopy in Geosciences, Part I: Basic Concepts of Crystal Field Theory*; EMU Notes in Mineralogy; Eötvös University Press: Budapest, Hungary, 2004; *Vol. 6*, p 93.
(32) Henderson, B.; Gallagher, H. G.; Han, T. P. J.; Scott, M. A. *J. Phys.: Condens. Matter* **2000**, *12*, 1927.
(33) Grinberg, M.; Sikorska, A.; Sliwinski, A.; Barzowska, J.; Shen, Y. R.; Ubizskii, S. B.; Melnyk, S. S. *Phys. Rev. B* **2003**, *67*, 045113.
(34) Shannon, R. D. *Acta Crystallogr.* **1976**, *A32*, 751.
(35) Hoppe, R. *Z. Kristallogr.* **1979**, *150*, 23.
(36) Hoppe, R.; Voigt, S.; Glaum, H.; Kissel, J.; Müller, H. P.; Bernet, K. *J. Less-Common Met.* **1989**, *156*, 105.
(37) Taran, M. N.; Langer, K.; Platonov, A. N.; Indutny, V. V. *Phys. Chem. Miner.* **1994**, *21*, 360.
(38) Langer, K.; Taran, M. N.; Platonov, A. N. *Phys. Chem. Miner.* **1997**, *24*, 109.
(39) König, E.; Kremer, S. *Ligand field energy diagrams*; Plenum Press: New York, 1977.
(40) Lenglet, M.; Hochu, F. *Mater. Res. Bull.* **2000**, *32*, 863.
(41) Juhin, A.; Calas, G.; Cabaret, D.; Galoisy, L.; Hazemann, J.-L. *Am. Mineral.* **2008**, *93*, 800.
(42) Juhin, A.; Calas, G.; Cabaret, D.; Galoisy, L.; Hazemann, J.-L. *Phys. Rev. B* **2007**, *76*, 054105.
(43) Gaudry, É.; Kiratisin, A.; Sainctavit, Ph.; Brouder, Ch.; Mauri, F.; Ramos, A.; Rogalev, A.; Goulon, J. *Phys. Rev. B* **2003**, *67*, 094108.
(44) Shannon, R. D.; Fischer, R. X. *Phys. Rev. B* **2006**, *73*, 235111.
(45) Garcia-Lastra, J. M.; Aramburu, J. A.; Barriuso, M. T.; Moreno, M. *Phys. Rev. B* **2006**, *74*, 115118.
(46) Moreno, M.; Garcia-Lastra, J. M.; Aramburu, J. A.; Barriuso, M. T. *Theor. Chem. Acc.* **2007**, *118*, 665.
(47) Garcia-Lastra, J. M.; Buzaré, J. Y.; Barriuso, M. T.; Aramburu, J. A.; Moreno, M. *Phys. Rev. B* **2007**, *75*, 155101.
(48) Dalconi, M. C.; Ardit, M.; Cruciani, G.; Blosi, M.; Dondi, M.; Albonetti, S. In preparation.

JP9043072